PG
Petroleum Geoscience

Research article

Published online August 31, 2017

https://doi.org/10.1144/petgeo2017-045 | Vol. 24 | 2018 | pp. 208–217

Two-step wireline log analysis of overpressure in the Bekapai Field, Lower Kutai Basin, Indonesia

Agus M. Ramdhan[1]* & Neil R. Goulty[2]

[1] Department of Geology, Institut Teknologi Bandung, Jl. Ganesha 10, Bandung 40132, Indonesia
[2] Department of Earth Sciences, Durham University, South Road, Durham DH1 3LE, UK
* Correspondence: agusmr@gc.itb.ac.id

Abstract: As part of our effort to improve pore-pressure estimation in diagenetically altered mudstones, we have used wireline logs to estimate disequilibrium compaction and unloading contributions to the hard overpressure encountered in the Bekapai Field, Lower Kutai Basin. The maximum vertical effective stress that the overpressured mudstones have experienced is estimated from the density log using Dutta's relationship between vertical effective stress and void ratio. The sonic–density cross-plot is then used to estimate the sonic reference trend: that is, the expected sonic response if the mudstones were currently at maximum vertical effective stress. Finally, comparison of the sonic log with the sonic reference trend gives the unloading contribution to overpressure using Bowers' unloading relationship between the vertical effective stress and velocity. In spite of poor data quality, fair results were obtained showing a steady increase in disequilibrium compaction overpressure below the top of the sharp pressure ramp. Immediately below the pressure ramp, the unloading contribution to overpressure dominates, with gas generation being the most likely cause. Our interpretation explains the pressure and wireline log data in this deltaic setting satisfactorily, resolving a debate on overpressure-generation mechanisms in the shelfal area of the basin that has been ongoing for 25 years.

Received 11 April 2017; **revised** 26 June 2017; **accepted** 10 July 2017

The Lower Kutai Basin is located in eastern Kalimantan (Fig. 1) and is the largest basin in Indonesia for gas production. The onshore area and the shelfal area surrounding the Mahakam Delta are mature areas for hydrocarbon exploration and production. In the shelfal area, fields are located along three major anticlines lying parallel to the coast, known as the Internal, Median and External axes. The Bekapai oil and gas field lies on the Median Axis. The sediments hosting and overlying the hydrocarbon accumulations are deltaic deposits sourced by the Mahakam River (Moss & Chambers 1999), and sedimentation has been continuous during the Neogene (Duval *et al.* 1998) so the strata are at maximum burial.

Due to lateral drainage through the deltaic sandstones, the pore pressure remains hydrostatic to depths of approximately 3 – 4 km below sea level, where there is a sharp pressure ramp into hard overpressure. Hydrocarbons are trapped hydrodynamically in the adjacent Peciko and Tunu fields (Grosjean *et al.* 2009), so it is probable that lateral water flow is also taking place in the overpressured reservoirs of the Bekapai Field.

Rapid burial during the Neogene was thought by earlier researchers to have generated the overpressure by disequilibrium compaction (Burrus *et al.* 1992; Bois *et al.* 1994; Bates 1996; Burrus 1998). Although doubts had been expressed about the quality of the density logs, the low mudstone porosities observed in the zone of hard overpressure are inconsistent with the disequilibrium compaction mechanism. These low porosities prompted Schneider *et al.* (1993) and Burrus (1998) to suggest that compaction depends on the Biot effective stress. Goulty (1998) argued that use of the Biot effective stress was inappropriate, and proposed that porosity should be related to mean effective stress instead of the vertical effective stress. However, in that paper he used poroelasticity and ignored soil mechanics principles: that is, during compaction, the void ratio depends on both mean effective stress and differential stress, although use of vertical effective stress is justified provided that the ratio between the horizontal effective stresses and the vertical effective stress does not change much with depth (Goulty 2004; Hauser *et al.* 2014).

In previous articles (Ramdhan & Goulty 2010, 2011), we have suggested that overpressure has been generated by unloading processes, especially gas generation, because mudstone density trends continue to increase downwards through the pressure ramp and the depth to top of hard overpressure coincides with the vitrinite reflectance threshold for gas generation. Furthermore, we suggested that the density reversal observed in the deepest well below the sharp pressure ramp was a consequence of 'chemical undercompaction', a process in which porosity was preserved by very high pore pressure holding pores open while the mudstone matrix was being cemented by the products of clay diagenesis (Goulty *et al.* 2012). We no longer think that chemical undercompaction is the correct explanation because it has become clear that diagenetically altered siliciclastic mudstones continue to compact mechanically in response to increasing effective stress (Cicchino *et al.* 2015; Goulty *et al.* 2016).

We have now applied two-step analysis to density and sonic logs at Bekapai to discriminate between loading and unloading mechanisms of overpressure generation. Our analysis method builds on the work of Bowers (1995, 2001), Dutta (1986, 2002, 2016) and Sargent *et al.* (2015). We find that although overpressure immediately below the onset of the sharp pressure ramp has predominantly been generated by unloading, the contribution of disequilibrium compaction gradually increases with depth. We claim that our interpretation finally makes sense of the pressure and wireline log data in this deltaic setting, resolving conflicting suggestions about overpressure generation mechanisms in the shelfal area of the Lower Kutai Basin.

We start with a brief review of the geology and overpressure regime in the Lower Kutai Basin. Then we describe the two-step method of wireline log analysis, and show the result of its application to two Bekapai wells that penetrate the pressure ramp into hard overpressure.

Geology

The development of the Kutai Basin has been described by Moss & Chambers (1999) and Chambers *et al.* (2004). Basin initiation took

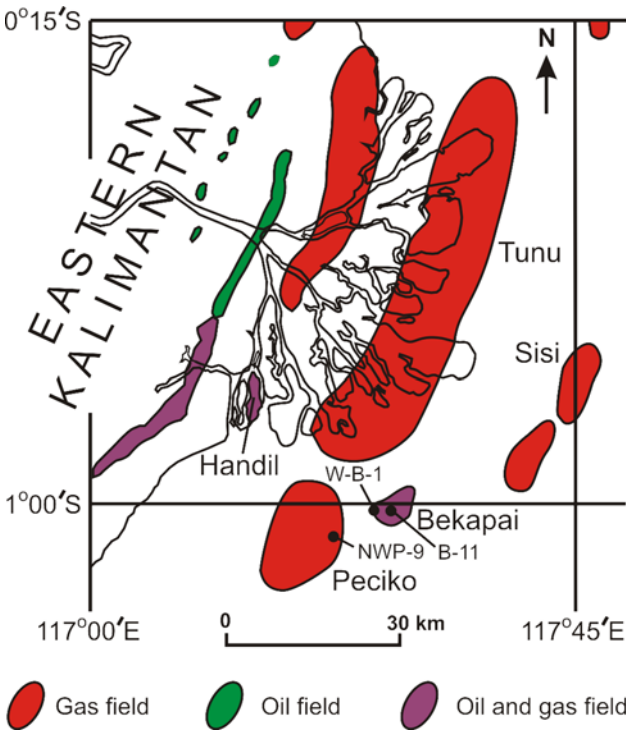

Fig. 1. Map of the Lower Kutai Basin showing fields and wells referred to in the text.

place during the middle–late Eocene as a consequence of tectonic extension in the SE Asia region (e.g. Hall 2009). The subsequent sag phase from the latest Eocene to the late Oligocene was marked by deposition of deep-marine muds in the basin centre. Early development of deltaic sediments occurred from the latest Oligocene to the early Miocene, with a second phase of tectonic extension in the basin centre. From the middle Miocene to the present, delta progradation has occurred, accompanied by the development of the Samarinda Anticlinorium which includes three anticlinal axes forming structural traps for hydrocarbons in the shelfal area of the Lower Kutai Basin (Fig. 1). Consequently, the Neogene strata in the shelfal area mainly comprise intercalated sandstones, mudstones and coals of the deltaic facies.

The hydrocarbons that have been produced in the Kutai Basin have come from the fluvio-deltaic petroleum system of middle Miocene–Pliocene age. A complete synthesis of this petroleum system was made by Paterson *et al.* (1997) and Duval *et al.* (1998), and a schematic model is shown in Figure 2. The main source rocks are organic-rich mudstones, coal beds and even sandy facies deposited in fluvial, delta-top, tidal-plain and delta-front settings, mostly classified as Type III source rocks. Although the organic-rich mudstones are gas-prone, Lambert *et al.* (2003) reported that the oil-generative potential of the Type III organic matter is unusually high. The contribution to hydrocarbon generation of the marine mudstones, located in the deeper part of the Neogene sequence, is thought to be negligible because their organic content is low. Interestingly, isotopic analysis performed by Lambert *et al.* (2003) showed that the threshold for both oil and gas generation corresponds to a vitrinite reflectance of 0.6%.

The reservoirs are fluvial and mouth-bar sandstones, and the seals are marine mudstones that developed during transgressions. Paterson *et al.* (1997) and Duval *et al.* (1998) proposed that hydrocarbons have predominantly migrated laterally from source rocks in the synclinal areas into the anticlinal traps.

The structure of the giant Bekapai oil and gas field is a faulted anticline with major faults striking approximately north–south, dividing the field into west, central and east compartments (Fig. 3). Production to date has been only from the west compartment. The stratigraphic interval that is the biggest contributor to hydrocarbon production from this field is the upper part of the Fresh Water Sand, deposited in the late Miocene (Fig. 4). The oil comes only from this zone. Other productive intervals for gas are the overlying Shallow Reservoir Zone of Pliocene age and the underlying Tunu Main Zone, also of late Miocene age. From the middle Miocene, the sedimentation rate at Bekapai has been fairly constant with an average rate of over 300 m Ma^{-1}. The top of overpressure in the west compartment is at depths of 3.0 – 3.5 km below sea level, where the temperature is 120 – 135°C.

Two-step method of analysis

For siliclastic mudstones in the shallow subsurface at temperatures below 65 – 70°C, where smectite starts to transform to illite, overpressure generated by disequilibrium compaction can be detected by an equivalent depth method using a sonic, resistivity or density log (Mouchet & Mitchell 1989). However, in the Lower Kutai Basin, we are concerned with diagenetically altered mudstones that may be overpressured by loading and unloading processes. We have used both density and sonic log responses in the mudstones to estimate the disequilibrium compaction and the unloading contributions to overpressure, the sum of the two being the total overpressure present.

The first step is to calculate from the density log values in the mudstones the maximum vertical effective stress to which the mudstones have been subjected. The maximum vertical effective stress the mudstones have experienced is subtracted from the present-day lithostatic stress, obtained by integrating the density log with respect to depth, to give the maximum loading pore pressure. Where the maximum loading pore pressure is greater than the hydrostatic pressure, the difference between the two may be thought of as the contribution to overpressure from disequilibrium compaction. Any additional overpressure is due to unloading mechanisms, such as gas generation, clay diagenesis and lateral transfer (Swarbrick *et al.* 2002).

Mudstones respond to unloading poroelastically. We assume that the poroelastic response of the density log is negligibly small, but unloading affects both sonic and resistivity logs significantly. Bowers & Katsube (2002) have suggested that decreasing normal effective stress opens flexible connecting pores of high aspect ratio sufficiently to affect transport properties without any significant effect on the bulk density of the mudstone. Thus, in the second step, we use the sonic log with an unloading velocity–effective stress relationship of the form proposed by Bowers (1995) to estimate the amount of unloading overpressure. Before doing so, we need to establish the sonic reference trend, which is the sonic response expected in the mudstones at their present depths if they were now at the maximum vertical effective stress they have previously experienced. If the wireline log data are of good quality, we are able to estimate the sonic reference trend for illitized mudstones using the sonic–density cross-plot.

Estimating maximum vertical effective stress

The relationship between vertical effective stress, σ'_v, and void ratio, e, for mechanical compaction given by Skempton (1969) is:

$$\sigma'_v = \sigma'_0 \exp(-\beta e) \quad (1)$$

where σ'_0 is the vertical effective stress when the void ratio is zero and β is a constant. Equation (1) was determined empirically from experimental data on clays and, as Skempton (1969) pointed out, only applies for values of vertical effective stress that are substantially less than σ'_0 because the void ratio must approach zero asymptotically at high vertical effective stress.

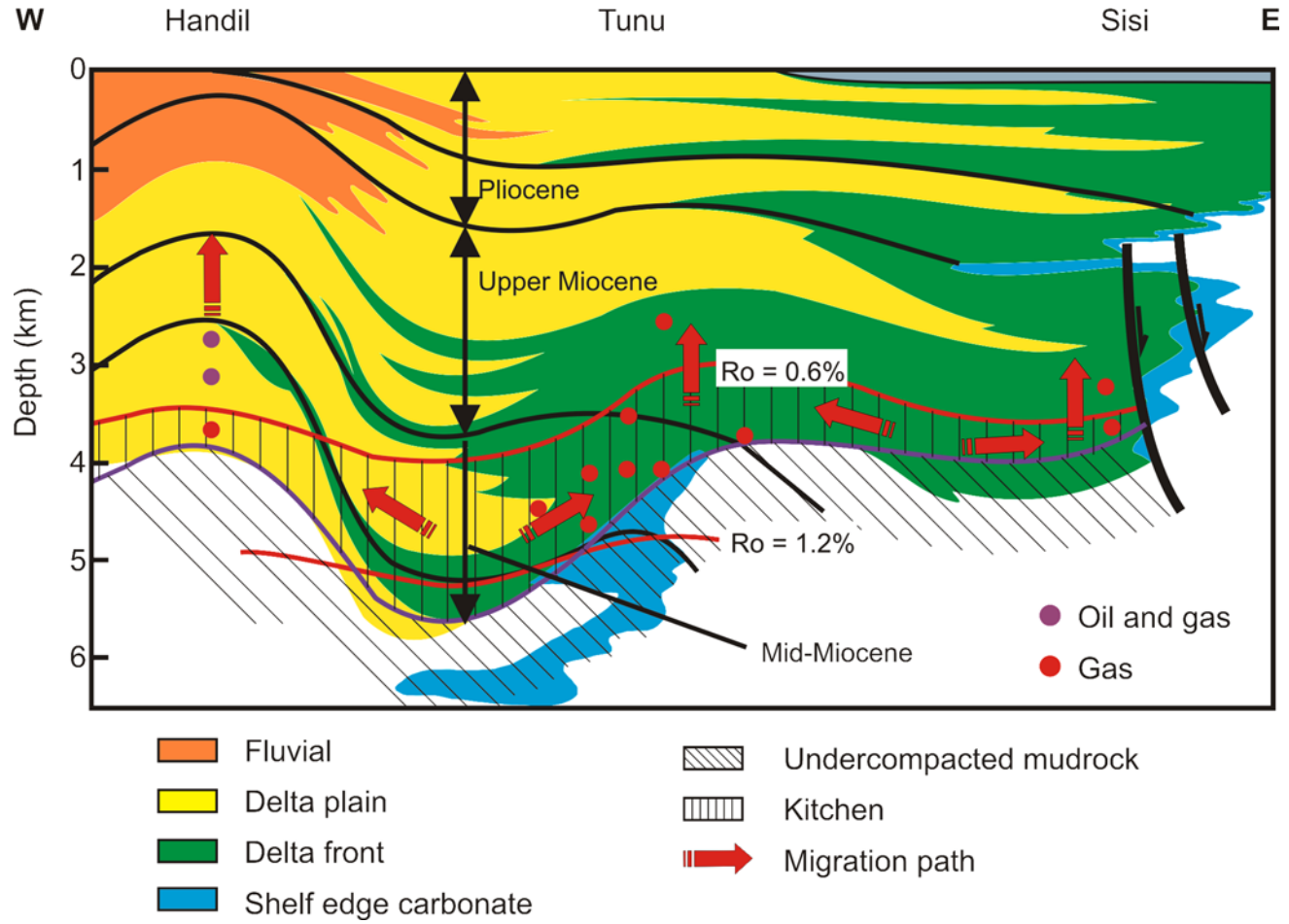

Fig. 2. Schematic cross-section of the Neogene petroleum system (simplified from Duval *et al.* 1998). The giant Bekapai oil and gas field lies approximately 10 km south of the supergiant Tunu gas field.

Dutta (1986, 2016) modified equation (1) by redefining β as the 'diagenesis function' to account for the mudstone's temperature history on the assumption that smectite–illite transformation occurs as a first-order kinetic reaction. We can use this modified relationship to estimate from the density log the maximum vertical effective stress experienced by diagenetically altered mudstones. The void ratio is obtained from the logged density in mudstone, ρ:

$$e = (\rho_s - \rho)/(\rho - \rho_f) \qquad (2)$$

where ρ_s is the density of the solid grains, assumed to be 2.75 g cm^{-3}, and ρ_f is the density of the pore fluid, assumed to be 1.05 g cm^{-3}.

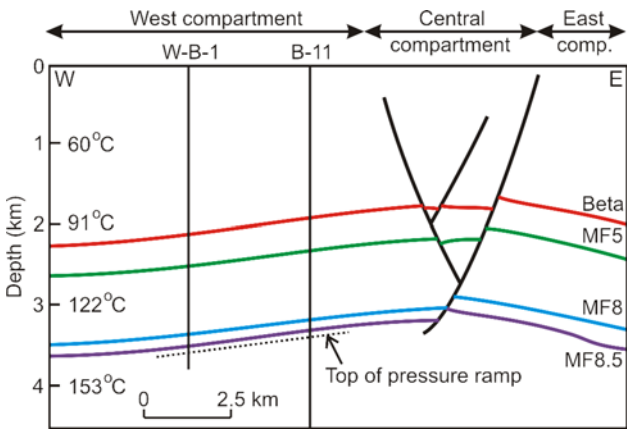

Fig. 3. Vertical section through the Bekapai Field.

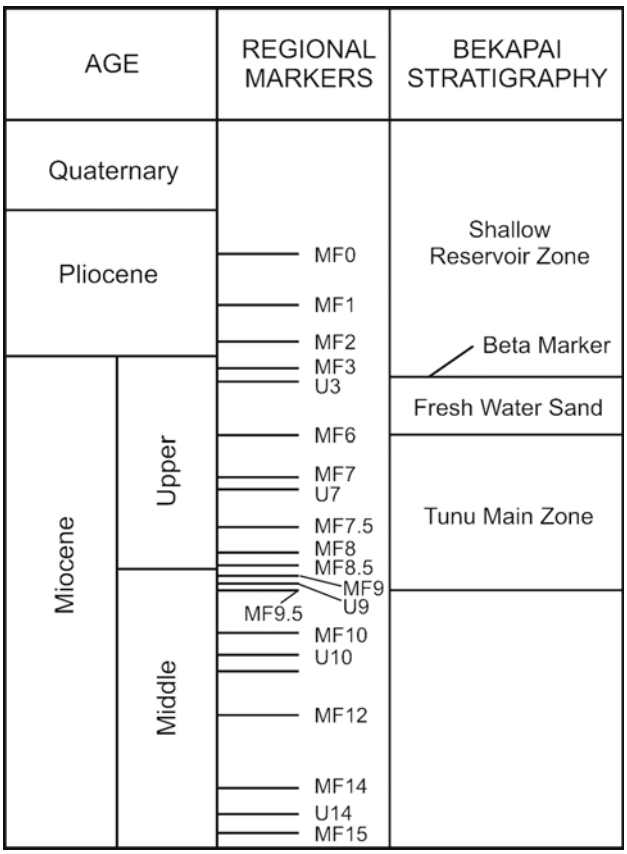

Fig. 4. Chronostratigraphic chart for the Bekapai Field.

The diagenesis function may be written as:

$$\beta = \beta_\infty - (\beta_\infty - \beta_0)\exp\left\{-\int_0^t A\exp\left[-E/RT(\tau)\right]\mathrm{d}\tau\right\} \quad (3)$$

where t is the depositional age of the bed concerned, β_∞ is the value the diagenesis function takes as $t \to \infty$, β_0 is the diagenesis function of the mudstone at deposition, τ is time since deposition, A is the Arrhenius frequency factor, E is the activation energy, R is the gas constant and T is temperature in degrees kelvin. Dutta (1986) determined the values of A and E from published X-ray diffraction (XRD) data for Gulf of Mexico mudstones as 40 000 a^{-1} and 80 750 J mol^{-1}, respectively, and later reported that these values were confirmed by using data from other basins (Dutta 2016). Taking logarithms of equation (1) and substituting for β from equation (3) yields:

$$\ln\sigma'_v + e\beta_\infty = \ln\sigma'_0 + e(\beta_\infty - \beta_0)\exp\left\{-\int_0^t A\exp[-E/RT(\tau)]\mathrm{d}\tau\right\} \quad (4)$$

We adopt the value of 9.4 for β_∞ given by Dutta (2016, his fig. 1) because he suggests it is applicable worldwide for siliciclastic mudstones in which illitization of smectite is complete. β_0 depends on the smectite composition of the mudstone at deposition, and has to be determined from the data. We estimate β_0 and σ'_0 from the gradient and intercept, respectively, of the best-fitting straight line on a plot of $\ln\sigma'_v + e\beta_\infty$ against $e \times \exp\{-\int_0^t A\exp[-E/RT(\tau)]\mathrm{d}\tau\}$ for data points in hydrostatically pressured mudstones, selected where the density log data quality is good.

If necessary, offset well data can also be used to assist in the estimation of β_0 and σ'_0. Other parameters required are the seafloor temperature, the geothermal gradient and the burial rate. In general, these three parameters may have varied over time, but we assumed constant values for the two Bekapai wells analysed below. Thus, given the density log, we have all the information needed to calculate from equation (1) the maximum vertical effective stress that has been experienced by mudstones in the deeper overpressured section of each well.

Estimating the sonic reference trend

The link between the two steps in our wireline log analysis method is provided by the sonic–density cross-plot. Dutta (2002) presented a cross-plot of sonic transit time and density for mudstones in the Gulf of Mexico. The black curve marked with arrows in Figure 5 approximates the average trend of his data, comprising a linear early compaction trend for smectite-rich mudstones and a linear late compaction trend for illite-rich mudstones, joined by a transitional section.

Amongst clay diagenetic reactions, the transformation of smectite to illite has the most influence on the compaction of mudstones in the depth range of interest. The reaction depends on both temperature and time. The onset of the transitional section of the arrowed curve in Figure 5 starts at approximately 70°C and the linear late compaction trend typically starts at some temperature in the range 90 – 100°C. Consequently, the transitional section is displaced to greater sonic travel time for a given density in basins with higher geothermal gradients or slower burial rates, and vice versa.

If mudstones become overpressured by disequilibrium compaction during burial, progress along the compaction trend on the cross-plot slows, and also deviates in the transitional section because the normal reduction in porosity with depth is inhibited when porewater cannot escape quickly enough for the pore pressure to remain in hydrostatic equilibrium. For illitized mudstones on the late compaction trend, we follow Sargent *et al.* (2015) in assuming that disequilibrium compaction would slow progress along that trend without deviation from it.

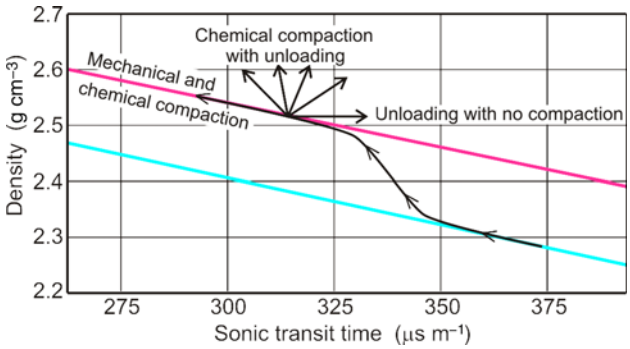

Fig. 5. Mudstone compaction trend (arrowed curve) on a sonic–density cross-plot based on results obtained by Dutta (2002) in the Gulf of Mexico. The trend is followed by mudstones undergoing progressive burial and compaction without unloading. The lower and upper parallel straight lines are Dutta's (2002) early and late trends for smectite-rich and illite-rich mudstones, respectively. The fan of arrows indicates possible paths for a diagenetically altered mudstone to follow, ranging from ongoing diagenesis without unloading to unloading without compaction.

If the vertical effective stress acting on a mudstone decreases at any stage of compaction, the resulting poroelastic unloading effect increases the sonic travel time whilst having negligible effect on bulk density. Then the mudstone's path on the sonic–density cross-plot would be towards the right. Unloading may be brought about by pore-pressure increases, whether due to fluid influx caused by gas generation, or lateral or vertical transfer, or due to clay diagenesis in mudstones which are so well sealed that porewater cannot escape. The combination of ongoing burial and diagenesis with partial inhibition of water escape, sufficient for the vertical effective stress to decrease with increasing burial depth, causes a mudstone's path on the cross-plot to lie somewhere on the arc between the late compaction trend and the unloading response for no compaction (Fig. 5).

Compaction trends for mudstones on the sonic–density cross-plot exhibit higher transit times for a given density with increasing clay content (Katahara 2003, 2006). To improve the consistency of the trends on the cross-plots, we applied log-based corrections to the sonic logs to take account of variations in the clay content of the mudstones, as described by Goulty *et al.* (2016). These lithology corrections were derived by correlating deviations from their smoothed trends of the sonic and natural gamma logs, and the difference between neutron and density porosity (NPHI – DPHI) computed from the density and neutron logs. Optimum multipliers for the gamma-ray and NPHI – DPHI deviations were found by simultaneous least squares to obtain the best fit to the sonic log deviations, assuming that the dependence is linear. The corrections thus generated were applied to the sonic log.

At Bekapai, we are only concerned with mudstones that lie on the late compaction trend on the sonic–density cross-plot, so this linear trend has to be estimated from the data above the top of overpressure. Following Sargent *et al.* (2015), we assume it is of the form:

$$\Delta t = \Delta t_L - 656\rho \quad (5)$$

where Δt is the sonic transit time in units of μs m^{-1} and ρ is density in units of g cm^{-3}. The gradient is fixed at the value given by Dutta (2002, his fig. 2) and the intercept on the sonic transit time axis, Δt_L, is determined from data in the subject well or, if necessary, from offset wells. Care must be taken because the intercept can differ

even between near-neighbour wells, as Sargent *et al.* (2015) found, probably because of differences in the environmental corrections applied to the density logs for hole size, mud type and temperature.

At each depth sample, the smoothed observed density is related to the maximum vertical effective stress through equation (1) and to the corresponding sonic transit time through equation (5), the late compaction trend on the sonic–density cross-plot. Hence, density can be eliminated between the two to give the notional sonic transit time corresponding to the maximum vertical effective stress experienced at each mudstone depth sample. This depth trend is the sonic reference trend.

Estimating the amount of unloading

To estimate the total pore pressure in mudstone using the two-step approach, we need the maximum loading pore pressure obtained from the density log in the first step, the sonic reference trend, and an unloading relationship between sonic velocity and vertical effective stress. Unloading shifts sonic transit time to higher values (i.e. reduces the sonic velocity), and we have adopted the following empirical power-law relationship for unloading proposed by Bowers (1995):

$$\sigma'_{\mathrm{v}} = \sigma'_{\mathrm{max}} \left[\frac{V - 1500}{V_{\mathrm{R}} - 1500} \right]^{U} \qquad (6)$$

where V is the observed sonic velocity and V_{R} is the velocity on the sonic reference trend in units of m s^{-1}, and U is the unloading velocity exponent. The total pore pressure is then found by subtracting σ'_{v} from the lithostatic stress.

Results

Most of the exploration wells drilled in the shelfal area of the Lower Kutai Basin terminated above the sharp pressure ramp, and others terminated within it. Hole conditions in many of the wells were poor due to the use of water-based drilling muds. Of the few wells that reached the pressure ramp, only two, W-B-1 and B-11 in the Bekapai Field, have density logs in the deeper part of each well that are adequate for our analysis.

West Bekapai-1 (W-B-1) well

The density log data are unreliable down to approximately 2400 m, so the lithostatic stress was taken to be the same as that in offset well NWP-9 in the Peciko Field down to 2500 m. NWP-9 is hydrostatically pressured down to 3300 m, and log quality is good because the well was drilled with oil-based mud. At depths below 2500 m in well W-B-1, the additional lithostatic stress was calculated from the W-B-1 density log.

Mudstone data were selected using data windows of 60 – 100 API units for the natural gamma log, and 0.05 – 0.18 for the difference in fractional porosity calculated from the neutron and density logs (NPHI − DPHI) (Fig. 6a). After data selection, the density log was smoothed using a 100 m-long Hanning (cosine-bell) window (Fig. 6b).

To determine the maximum vertical effective stress experienced by the mudstones from equation (1), we estimated β_0 as 8.66 ± 0.08 and σ'_0 as 121.8 ± 0.8 MPa by the method described above, where the errors are expressed at the ±1 SD confidence level, based on equation (4). We determined the gradient and intercept of the best-fitting straight line for the hydrostatically pressured mudstone data points in the depth range 2400 – 3500 m (Fig. 7a), where the density log quality is good (Fig. 7b). The resultant density normal compaction trend, extrapolated to the bottom of the well assuming hydrostatic pore pressure, is superimposed on the density data in Figure 7b. It overlies the density data to the bottom of the well, strongly suggesting that there is no overpressure generated by disequilibrium compaction because there is no anomalous porosity.

Our value of β_0 is significantly larger than the value 6.6 given by Dutta (2016, his fig. 1). We attribute our larger value to a lower initial smectite content in the Lower Kutai Basin mudstones compared to those investigated by Dutta (2016), which would be consistent with the XRD analysis of the clay mineral fraction in the Handil and Tunu fields (Clauer *et al.* 1999). Other parameters were: seafloor temperature 30°C; constant geothermal gradient of 31°C km^{-1}; and constant burial rate of 350 m Ma^{-1} estimated from the ages of key horizons given by Lambert *et al.* (2003). Hence, the diagenesis function, β, was found for all depths using equation (3). The mudstone void ratio was calculated from the smoothed density log (Fig. 6b).

The sonic, NPHI − DPHI and natural gamma values logged in the mudstones were also smoothed using the 100 m-long Hanning window. Deviations from the smoothed log trends were calculated, and correction factors for the sonic log deviations were estimated by least squares using the NPHI − DPHI and natural gamma deviations as independent variables. The sonic log for the selected mudstone data points with corrections for clay content applied is shown in Figure 6c.

From a visual comparison of the density and corrected sonic logs with the pressure–depth plot (Fig. 6d), it is possible to identify a reversal in the sonic log around the top of the sharp pressure ramp at 3600 m depth, but not in the density log. The sonic–density cross-plot of the smoothed logs (Fig. 6e) emphasizes the reversal in sonic transit time. Hydrostatically pressured data over the depth interval 2450 – 3500 m were used to find the intercept in equation (5), where the linear late compaction trend for illite-rich mudstones at maximum vertical effective stress meets the sonic transit time axis on the cross-plot, as $\Delta t_{\mathrm{L}} = 1941$ μs m^{-1}.

The maximum loading pore pressure, corresponding to the maximum vertical stress, was estimated from the smoothed density log using equation (1) (Fig. 6d). The total pore pressure was then calculated from equation (6) using the smoothed sonic log of Figure 6c and the sonic reference trend, obtained from the smoothed density log and equation (5). The choice of 4.5 for the unloading exponent in equation (6) gives a fair fit, overall, to the measured pore pressures and mud-weight profile (Fig. 6d).

Bekapai-11 (B-11) well

The density log data are unreliable down to 3491 m, so the lithostatic stress was taken to be the same as that in offset well NWP-9 in the Peciko Field down to 3500 m. At greater depths, additional lithostatic stress was calculated from the density log in B-11.

Mudstone data were selected using data windows of 40 – 90 API units for the natural gamma log, and 0.08 – 0.2 for the difference in fractional porosity calculated between the neutron and density logs (NPHI − DPHI) (Fig. 8a). After data selection, the logs were smoothed using a 100 m-long Hanning window.

To determine the maximum vertical effective stress experienced by the mudstones using equation (1), we assumed $\beta_0 = 8.66$, as in well W-B-1. From the values of β, hydrostatic vertical effective stress and the smoothed void ratio at 3500 m depth in well B-11, the constant σ'_0 was estimated to be 107.9 MPa. This value differs from the value of σ'_0 determined in well W-B-1 mainly because of the difference in logged density between the two wells, which is probably a consequence of pore hole conditions and differences in the way that environmental corrections were applied. Other parameters were: seafloor temperature 30°C; constant geothermal gradient of 31°C km^{-1}; and constant burial rate of 330 m Ma^{-1} estimated from the ages of key horizons given by Lambert *et al.* (2003). Hence, the diagenesis function, β, was found for all depths

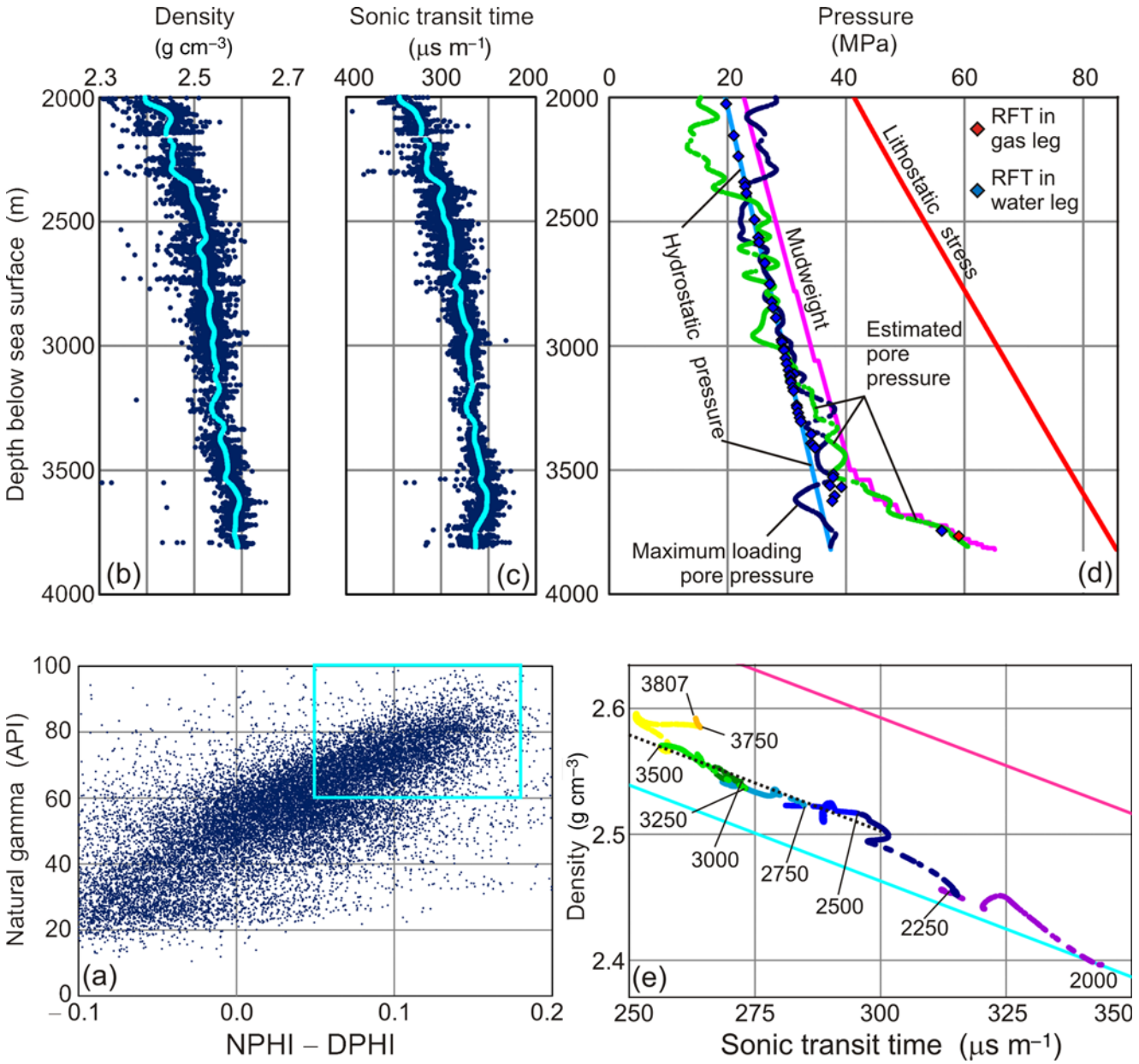

Fig. 6. Data from well W-B-1. (**a**) Cross-plot of natural gamma against NPHI − DPHI for all data points below 2000 m. The box indicates selected mudstone data points. (**b**) Density log with smoothed log. (**c**) Sonic log corrected for clay content with smoothed log. (**d**) Pressure–depth plot with estimates of the maximum loading pore pressure and the total pore pressure. (**e**) Sonic–density cross-plot using the smoothed logs. Sticks mark depths in metres. The solid, parallel straight lines are Dutta's (2002) early and late trends for smectite-rich and illite-rich mudstones, only included here as reference lines. The dotted line is the late compaction trend picked for illite-rich mudstones at maximum vertical effective stress.

using equation (3). The mudstone void ratio was calculated from the smoothed density log (Fig. 8b).

The sonic log was corrected for clay content as before, using log data below 3491 m only for calculating the corrections, and the whole corrected log was smoothed (Fig. 8c). From visual comparison of the density and corrected sonic logs with the pressure–depth plot (Fig. 8d), a strong reversal in the sonic log can be identified at a depth of approximately 3300 m, around the top of the sharp pressure ramp, and a reversal in density can be picked at approximately 3650 m depth, close to the base of the sharp pressure ramp.

To obtain the sonic–density cross-plot (Fig. 8e), the smoothed density log was used only below 3491 m. At shallower depths, the density normal compaction trend was used (Fig. 8b), calculated from the values of β and hydrostatic vertical effective stress with $\sigma'_0 = 107.9$ MPa. The cross-plot is suspect at depths shallower than 3491 m because the smooth density normal compaction trend has been used there and the poor hole conditions in well B-11 have affected the sonic log. The quality of both sonic and density logs in well B-11 is poor over the depth range 2500 – 3500 m compared with well W-B-1 (Figs 6b, c and 8b, c), so the linear late compaction trend on the sonic–density cross-plot for illite-rich mudstones at maximum vertical effective stress in B-11 could not be estimated satisfactorily from the data, and was assumed to be the same as in W-B-1. In spite of the problems with the shallower log data, the sonic–density cross-plot emphasizes the reversal in the sonic log and, at a greater depth, the reversal in the density log.

The maximum loading pore pressure, corresponding to the maximum vertical stress, was estimated from the smoothed density log using equation (1), and increases downwards in an approximately linear manner below 3600 m depth (Fig. 8d). The total pore pressure was then calculated from equation (6) using the smoothed sonic log of Figure 8c and the sonic reference trend, using the same value of 4.5 for the unloading exponent U as estimated in well W-B-1.

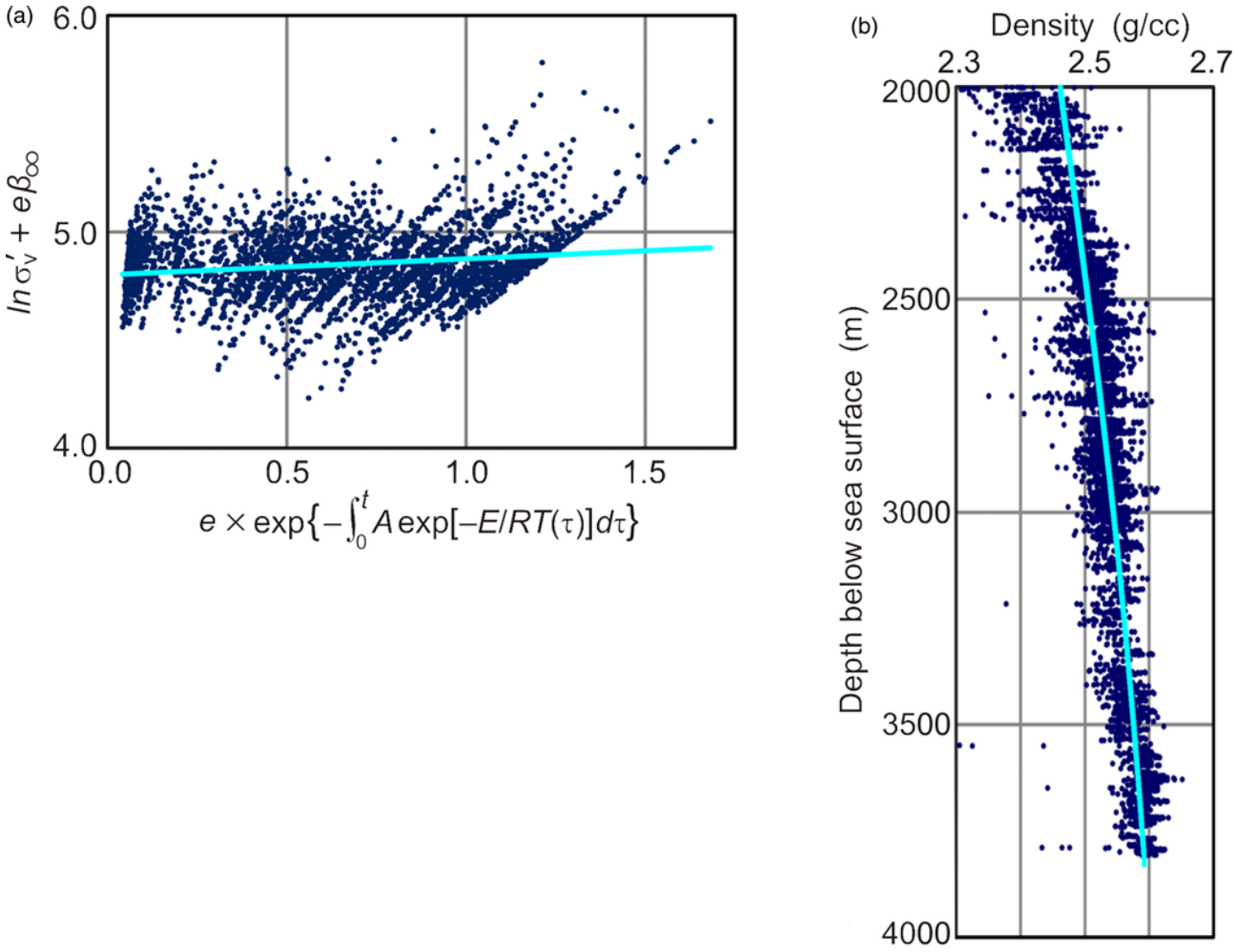

Fig. 7. (**a**) Plot based on equation (4) to estimate β_0 and σ_0' for the hydrostatically pressured mudstone data points in well W-B-1 over the depth range 2400 – 3500 m. The gradient is $\beta_\infty - \beta_0 = 0.74 \pm 0.08$, yielding $\beta_0 = 8.66 \pm 0.08$ for the assumed value of $\beta_\infty = 9.4$. The intercept is $\ln \sigma_0' = 4.8026 \pm 0.0061$, yielding $\sigma_0' = 121.8 \pm 0.8$ MPa. (**b**) Mudstone density data from well W-B-1 overlain by the density normal compaction trend for hydrostatic vertical effective stress, found from equation (1) with parameters determined from the plot in (a).

Interpretation

The density log quality in well W-B-1 is poor at depths shallower than 2400 m. Consequently, the estimated maximum loading pore pressure and total pore pressure at the shallowest depths in Figure 6d should be ignored. At greater depths, short-wavelength fluctuations in the smoothed density log result in short-wavelength fluctuations in the maximum loading pore pressure: e.g. high density around 3600 m depth causes the estimated maximum loading pore pressure to be less than hydrostatic pressure. Abnormally high density leads to abnormally low sonic transit time on the sonic reference trend and, consequently, overestimation of the amount of unloading overpressure. In some parts of both wells, notably in B-11 (Fig. 8d), these effects cancel each other out to give a good estimate of the pore pressure, but in others they do not. There are also short-wavelength fluctuations in the smoothed sonic logs, in spite of the corrections for clay content, that do not correlate with the density logs: for example, over the depth range 2400 – 3500 m in W-B-1 where the pore pressure is hydrostatic (Fig. 6b, c). We attribute these fluctuations primarily to variations in mudstone lithology, although log data quality might also be an issue.

Nevertheless, the pressure trends for maximum loading pore pressure and total pore pressure below the top of the sharp pressure ramp in each well are broadly consistent between the two wells. Furthermore, the pressure trends are consistent with the reversals seen on the sonic log in W-B-1 (Fig. 6c, e), and on both density and sonic logs in B-11 (Fig. 8b, c, e). We attribute the reversal on the density log at approximately 3650 m depth in B-11 to disequilibrium compaction, and the reversals on the sonic logs in both wells to unloading. Disequilibrium compaction enhances the sonic reversal below 3650 m depth in B-11.

In the shelfal area of the Lower Kutai Basin, the top of the sharp pressure ramp into hard overpressure is found within upper Miocene strata at depths of 3 – 4 km and, with the exception of the neighbourhood of the Handil Field (Fig. 1), these strata are at maximum burial. In almost every field in the shelfal area, the depth of the top of the pressure ramp varies and cross-cuts stratigraphic boundaries. In such circumstances, the mechanisms of overpressure generation that are most likely to cause a significant amount of unloading are clay diagenesis and gas generation (Swarbrick *et al.* 2002).

Transformation of smectite to illite starts at around 65 – 70°C and is the principal clay diagenetic change in mudstones up to approximately 120°C. The reaction pathways release water, silica and cations that can react with kaolinite and calcite to produce chlorite and ankerite (Boles & Franks 1979). When mudstones have attained a temperature of approximately 120°C through burial, the proportion of expandable 'smectitic' interlayers containing hydrated cations in mixed-layer illite–smectite crystals has generally reduced to about 20% with all the smectite 2:1 layers having dissolved, so that the remaining expandable interlayers separate illite fundamental particles (Środoń *et al.* 2000).

In the shelfal area of the Lower Kutai Basin, the temperature of 120°C is reached by 3 km depth, whereas the top of the sharp pressure

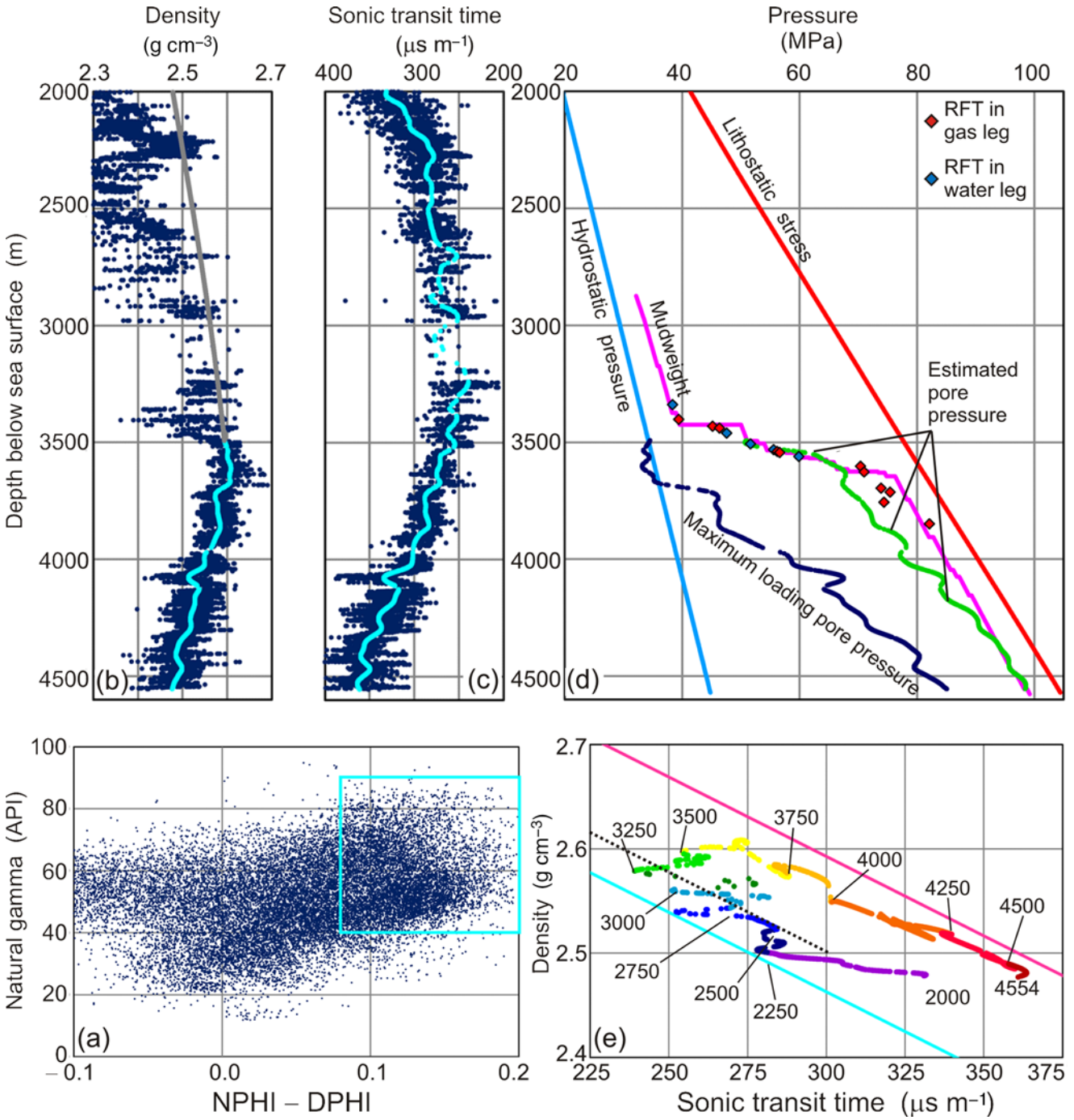

Fig. 8. Data from well B-11. (**a**) Cross-plot of natural gamma against NPHI – DPHI for all data points below 2000 m. The box indicates selected mudstone data points. (**b**) Density log with smoothed log below 3491 m. The smooth density trend above 3491 m was calculated from equation (1) using the diagenesis function and assuming hydrostatic vertical effective stress. (**c**) Sonic log corrected for clay content, with smoothed log. (**d**) Pressure–depth plot with estimates of the maximum loading pore pressure and the total pore pressure. (**e**) Sonic–density cross-plot using the smoothed logs in (b) and (c). Sticks mark depths in metres. The solid, parallel straight lines are Dutta's (2002) early and late trends for smectite-rich and illite-rich mudstones, only included here as reference lines. The dotted line is the late compaction trend estimated for illite-rich mudstones at maximum vertical effective stress.

ramp is located at approximately 3.5 km depth in the Bekapai Field. Although there are other diagenetic reactions in clays, such as the transformation of kaolinite into illite which continues above 120°C if a source of potassium is still available, smectite to illite transformation is the clay diagenetic reaction that has the greatest effect on mudstone compaction because of the disappearance of smectite and smectitic interlayers (Lahann 2002). Thus, clay diagenesis is probably not a major contributor to the unloading overpressure.

According to Lambert *et al.* (2003), gas generation starts in the Lower Kutai Basin at a vitrinite reflectance threshold of 0.6%. Vitrinite reflectance data from four fields, Sisi, Peciko, Handil and Nilam (Fig. 1), show that the threshold value of 0.6% coincides with the top of the sharp pressure ramp in the respective fields (Ramdhan & Goulty 2011). It seems likely, therefore, that gas generation is principally responsible for the unloading contribution to overpressure.

Discussion

In this section, we first summarize our two-step approach and emphasize how it differs from previously published approaches. Then we evaluate the effect of uncertainty in lithostatic stress, quantify the effect of neglecting the poroelastic effect of unloading on density and comment on the value of the unloading exponent estimated from the data in well W-B-1.

Our two-step analysis may be considered as a version of the method proposed by Bowers (2001), who was the first to use both density and sonic logs to estimate pore pressure where both disequilibrium compaction and unloading mechanisms have generated overpressure. The basis of the two-step approach is that we assume the density log is primarily sensitive to disequilibrium compaction overpressure, and that the sonic log is sensitive to both disequilibrium compaction overpressure and unloading overpressure.

We have adopted Dutta's (1986) relationship between vertical effective stress and void ratio to describe compaction, as defined by equations (1) and (3), to account explicitly for clay diagenesis. Void ratio is obtained directly from the observed density. In contrast, Bowers (2001) considered that mudstone compaction trends for both velocity and density depend only on vertical effective stress, and are independent of mudstone temperature history and diagenesis. We assume that the vertical effective stress calculated from equations (1) and (3) is the maximum vertical effective stress that the mudstone has experienced. This first step yields the maximum loading pore pressure, and thereby the disequilibrium compaction contribution to overpressure.

A key assumption we make is that mudstones that fall on the arrowed compaction curve on the sonic–density cross-plot (Fig. 5), and specifically on the linear late compaction trend for mudstones at temperatures above 100°C, are at the maximum vertical effective stress they have experienced, regardless of the relative contributions of mechanical and chemical compaction (Sargent *et al.* 2015). Hence, the arrowed curve provides the required link between the observed density and the sonic transit time at maximum vertical effective stress, yielding the sonic reference trend.

In the second step, we adopt the unloading relationship of equation (6) (Bowers 1995) between velocity and vertical effective stress to estimate the present-day vertical effective stress in the mudstones from the maximum vertical effective stress they have experienced. Unloading causes a reduction in the observed sonic transit time compared to the sonic transit time the same mudstone bed would have at the maximum vertical effective stress it has previously experienced. This second step differs from Dutta's (2016) methodology because he introduced the equation of Raiga-Clemenceau *et al.* (1988) to relate sonic transit time, or seismic slowness, directly to porosity, and hence to vertical effective stress through equations (1) and (2). His motivation was to estimate vertical effective stress from velocity alone, in order to estimate overpressure from the seismic velocity field computed from surface seismic reflection data, as described by Dutta *et al.* (2014). Unfortunately, the vertical effective stress acting on a mudstone of given lithology is not a single-valued function of velocity. The velocity increase due to a fixed increment of vertical effective stress during compaction is much smaller than the velocity reduction that occurs if unloading subsequently decreases the vertical effective stress by the same amount. For the same reason, methods of pore-pressure estimation using only the sonic log, such as the popular method of Eaton (1975), gives erroneous results where there are changes in the relative contributions of disequilibrium compaction and unloading to overpressure (Goulty & Sargent 2016).

For well W-B-1, we found that the value 4.5 for the unloading exponent U in equation (6) gave a reasonable fit to the measured pressures. Bowers (1995) found values of U (equivalent to U/B in his paper) to be about 3.8 for the Gulf Coast, 5.0 for the deep-water Gulf of Mexico and 5.6 for Jurassic mudstones in the Central North Sea, while Sargent *et al.* (2015) used $U = 1.5$ for Cretaceous mudstones at Haltenbanken, indicating a much greater sensitivity to unloading there. Hermanrud *et al.* (1998) had previously found that sonic velocity in the Jurassic Not Formation at Haltenbanken is also relatively sensitive to lateral variations in vertical effective stress. Teige *et al.* (2007) compared velocity–effective stress relationships in North Sea and Haltenbanken mudstones, and concluded that sonic velocity had a much greater sensitivity at Haltenbanken. The cause is unknown, although Teige *et al.* (2007) suggested that it might be due to microfracturing in response to crustal flexuring because progradation of thick Plio-Pleistocene sedimentary wedges, varying Quaternary ice loads at the shelf edge and uplift of mainland Norway in the Plio-Pleistocene resulted in more crustal flexuring at Haltenbanken than in the North Sea (Nordgård Bolås *et al.* 2005).

One possible source of error in the estimated contributions to overpressure from disequilibrium compaction and unloading is uncertainty in the lithostatic stress. Density logs are commonly not acquired at shallow depths, so assumptions have to be made about the shallow density–depth profile which may contribute a fixed error in overburden stress at greater depths. To estimate its effect, we repeated the analysis of the data in well W-B-1 assuming that the lithostatic stress had been underestimated by 1.0 MPa. Consequently, the value of the constant σ_0' in equation (1) increased, and both the density normal compaction trend and the sonic reference trend were altered. At 3807 m depth in well W-B-1, the greatest depth where data are available (Fig. 6b–d), the estimated disequilibrium compaction pore pressure reduced by 0.1 MPa, whereas the estimated total pore pressure increased by 0.4 MPa.

For simplicity, we have neglected the effect of poroelastic unloading on density, but it would be possible to allow for it. To check whether we are justified in neglecting the effect of poroelastic unloading on density, we estimated the magnitude of the effect at approximately 4300 m depth in well B-11. Using Gassmann theory for an isotropic medium, with mudstone sonic velocity and density values taken from the logs and assuming a Poisson's ratio of 0.28, we calculate that 30 MPa of overpressure causes a poroelastic increase in porosity of 0.37%. Correcting for this increase in porosity reduces the estimated contribution to pore pressure from disequilibrium compaction by 1.0 MPa. The estimated contribution to overpressure from unloading then increases by 1.5 MPa due to the consequent reduction of 4.1 μs m^{-1} in transit time on the sonic reference trend. Thus, neglect of the effect of poroelastic unloading on density at this depth in this well causes the pore pressure to be underestimated by about 0.5 MPa.

Given our interpretation that the unloading contribution to overpressure in the shelfal area of the Lower Kutai Basin is due to gas generation, we should consider whether the reversals in the sonic logs in the Bekapai wells are in part due to the presence of free gas. The resistivity log response in the mudstones reverses at the same depth as the sonic log (see fig. 8 in Ramdhan & Goulty 2011), whereas free gas would have the effect of increasing the resistivity, and the resistivity log has a greater depth of penetration into the formation than does the sonic log. Furthermore, the low sensitivity of the sonic log to unloading, with the values of the unloading exponent U similar to those determined by Bowers (2001) for the Gulf Coast and deep-water Gulf of Mexico, suggests that the unloading effect on the sonic response is not reinforced by the presence of free gas. However, the form of the unloading relationship in equation (6) is empirical and the value of 4.5 for the unloading exponent was chosen to fit the pressure data in well W-B-1; so although we have not identified a gas effect on sonic velocity, we cannot categorically rule it out.

Conclusions

We have used wireline logs to estimate disequilibrium compaction and unloading contributions to the hard overpressure encountered in the Bekapai Field, Lower Kutai Basin. Pressure profiles in this field are typical of those encountered in the shelfal area of the basin. In spite of poor data quality, fair results were obtained showing a steady increase in disequilibrium compaction overpressure below the top of the sharp pressure ramp. Immediately below the pressure ramp, the unloading contribution to overpressure dominates, with gas generation being the most likely mechanism. Our interpretation

explains the pressure and wireline log data in this deltaic setting satisfactorily, resolving a debate on overpressure generation mechanisms in the shelfal area of the basin that has been ongoing for 25 years.

Finally, we emphasize that the two-step analysis is useful for estimating the respective contributions to overpressure due to loading and unloading mechanisms but, because of its high sensitivity to variations in the density log response caused by lithological and environmental factors, it should be used with great care as a method of pore-pressure estimation. Log data quality is of crucial importance.

Acknowledgements We thank Total Indonesie for providing the data; Peter Andras, Andy Aplin, Alan Mitchell, Colin Sargent, Guillaume Smagghe and Richard Swarbrick for helpful discussions; and Nader Dutta and an anonymous reviewer for their constructive comments.

References

Bates, J.A. 1996. Overpressuring in the Kutai Basin: distribution, origins, and implications for the petroleum system. *In*: Proceedings of 25th Annual Convention, Indonesian Petroleum Association, Jakarta, 93–115.

Bois, M., Grosjean, Y. & de Pazzis, L. 1994. Shale compaction and abnormal pressure evaluation application to the offshore Mahakam. *In*: Proceedings of 23rd Annual Convention, Indonesian Petroleum Association, Jakarta, 245–259.

Boles, J.R. & Franks, S.G. 1979. Clay diagenesis in Wilcox Sandstones of southwest Texas: implications of smectite diagenesis on sandstone cementation. *Journal of Sedimentary Petrology*, **49**, 55–70.

Bowers, G.L. 1995. Pore pressure estimation from velocity data: accounting for overpressure other than undercompaction. *SPE Drilling & Completion*, **10**, 89–95.

Bowers, G.L. 2001. Determining an appropriate pore-pressure estimation strategy. Paper OTC-13042 presented at the Offshore Technology Conference, 30 April–3 May 2001, Houston, Texas.

Bowers, G.L. & Katsube, T.J. 2002. The role of shale pore structure on the sensitivity of wire-line logs to overpressure. *In*: Huffman, A.R. & Bowers, G.L. (eds) *Pressure Regimes in Sedimentary Basins and their Prediction*. American Association of Petroleum Geologists, Tulsa, OK, 43–60.

Burrus, J. 1998. Overpressure models for clastic rocks, their relation to hydrocarbon expulsion: a critical reevaluation. *In*: Law, B.E., Ulmishek, G.F. & Slavin, V.I. (eds) *Abnormal Pressures in Hydrocarbon Environments*. American Association of Petroleum Geologists, Tulsa, OK, 35–63.

Burrus, J., Brosse, E., Choppin de Janvry, G., Grosjean, Y. & Oudin, J.L. 1992. Basin modelling in the Mahakam Delta based on integrated 2D model Temispack. *In*: Proceedings of 21st Annual Convention, Indonesian Petroleum Association, Jakarta, 23–43.

Chambers, J.L.C., Carter, I., Cloke, R., Craig, J., Moss, S.J. & Paterson, D.W. 2004. Thin-skinned and thick-skinned inversion-related thrusting – a structural model for the Kutai Basin, Kalimantan, Indonesia. *In*: McClay, K.R. (ed.) *Thrust Tectonics and Hydrocarbon Systems*. American Association of Petroleum Geologists, Tulsa, OK, 614–634.

Cicchino, A.M.P., Sargent, C., Goulty N.R. & Ramdhan, A.M. 2015. Regional variation in Cretaceous mudstone compaction trends across Haltenbanken, offshore mid-Norway. *Petroleum Geoscience*, **21**, 17–34, https://doi.org/10.1144/petgeo2014-035

Clauer, N., Rinckenbach, T., Weber, F., Sommer, F., Chaudhuri, S. & O'Neil, J.R. 1999. Diagenetic evolution of clay minerals in oil-bearing Neogene sandstones and associated shales, Mahakam Delta Basin, Indonesia. *AAPG Bulletin*, **83**, 62–87.

Dutta, N.C. 1986. Shale compaction, burial diagenesis and geopressures: a dynamic model, solution and some results. *In*: Burrus, J. (ed.) *Thermal Modeling in Sedimentary Basins*. Éditions Technip, Paris, 149–172.

Dutta, N.C. 2002. Deepwater geohazard prediction using prestack inversion of large offset P-wave data and rock model. *The Leading Edge*, **21**, 193–198.

Dutta, N.C. 2016. Effect of chemical diagenesis on pore pressure in argillaceous sediment. *The Leading Edge*, **35**, 523–527.

Dutta, N.C., Yang, S., Dai, J., Chandrasekhar, S., Dotiwala, F. & Rao, C.V. 2014. Earth model building using rock physics and geology for depth imaging. *The Leading Edge*, **33**, 1136–1152.

Duval, B.C., Cassaigneau, C., Choppin de Janvry, G., Loiret, B., Leo, M., Alibi & Grosjean, Y. 1998. Impact of the petroleum system approach to exploration and appraisal efficiency in the Mahakam Delta. *In*: Proceedings of 26th Annual Convention, Indonesian Petroleum Association, Jakarta, 277–290.

Eaton, B.A. 1975. The equation for geopressure prediction from well logs. Paper SPE 5544 presented at the Fall Meeting of the Society of Petroleum Engineers of AIME, 28 September–1 October 1975, Dallas, Texas.

Goulty, N.R. 1998. Relationships between porosity and effective stress in shales. *First Break*, **16**, 413–419.

Goulty, N.R. 2004. Mechanical compaction behaviour of natural clays and implications for pore pressure estimation. *Petroleum Geoscience*, **10**, 73–79, https://doi.org/10.1144/1354-079302-552

Goulty, N.R. & Sargent, C. 2016. Compaction of diagenetically altered mudstones – Part 2: Implications for pore pressure estimation. *Marine and Petroleum Geology*, **77**, 806–818.

Goulty, N.R., Ramdhan, A.M. & Jones, S.J. 2012. Chemical compaction of mudrocks in the presence of overpressure. *Petroleum Geoscience*, **18**, 471–479, https://doi.org/10.1144/petgeo2012-018

Goulty, N.R., Sargent, C., Andras, P. & Aplin, A.C. 2016. Compaction of diagenetically altered mudstones – Part 1. Mechanical and chemical contributions. *Marine and Petroleum Geology*, **77**, 703–713.

Grosjean, Y., Zaugg, P. & Gaulier, J.-M. 2009. Burial hydrodynamics and subtle hydrocarbon trap evaluation: from the Mahakam Delta to the Caspian Sea. Paper IPTC 13962 presented at the International Petroleum Technology Conference, 7–9 December 2009, Doha, Qatar.

Hall, R. 2009. Hydrocarbon basins in SE Asia: understanding why they are there. *Petroleum Geoscience*, **15**, 131–146, https://doi.org/10.1144/1354-079309-830

Hauser, M.R., Couzens-Schultz, B.A. & Chan, A.W. 2014. Estimating the influence of stress state on compaction behavior. *Geophysics*, **79**, D389–D398.

Hermanrud, C., Wensas, L., Teige, G.M.G., Nordgård Bolås, H.M., Hansen, S. & Vik, E. 1998. Shale porosities from well logs on Haltenbanken (offshore mid-Norway) show no influence of overpressuring. *In*: Law, B.E., Ulmishek, G.F. & Slavin, V.I. (eds) *Abnormal Pressures in Hydrocarbon Environments*. American Association of Petroleum Geologists, Tulsa, OK, 65–85.

Katahara, K. 2003. Analysis of overpressure on the Gulf of Mexico Shelf. Paper OTC-15293 presented at the Offshore Technology Conference, 5–8 May 2003, Houston, Texas.

Katahara, K. 2006. Overpressure and shale properties: stress unloading or smectite–illite transformation? *In*: SEG Annual Meeting, *Expanded Abstracts*, 1520–1524.

Lahann, R. 2002. Impact of smectite diagenesis on compaction modelling and compaction equilibrium. *In*: Huffman, A.R. & Bowers, G.L. (eds) *Pressure Regimes in Sedimentary Basins and their Prediction*. American Association of Petroleum Geologists, Tulsa, OK, 61–72.

Lambert, B., Duval, B.C., Grosjean, Y., Umar, I.M. & Zaugg, P. 2003. The Peciko case history: impact of an evolving geological model on the dramatic increase of gas reserves in the Mahakam Delta. *In*: Halbouty, M.T. (ed.) *Giant Oil and Gas Fields of the Decade 1990–1999*. American Association of Petroleum Geologists, Tulsa, OK, 297–320.

Moss, S.J. & Chambers, J.L.C. 1999. Depositional modelling and facies architecture of rift and inversion episodes in the Kutai Basin, Kalimantan, Indonesia. *In*: Proceedings of 27th Annual Convention, Indonesian Petroleum Association, Jakarta, 467–486.

Mouchet, J.P. & Mitchell, A. 1989. *Abnormal Pressures while Drilling*. Éditions Technip, Paris.

Nordgård Bolås, H.M., Hermanrud, C. & Teige, G.M.G. 2005. The influence of stress regimes on hydrocarbon leakage. *In*: Boult, P. & Kaldi, J. (eds) *Evaluating Fault and Cap Rock Seals*. American Association of Petroleum Geologists, Tulsa, OK, 109–123.

Paterson, D.W., Bachtiar, A., Bates, J.A., Moon, J.A. & Surdam, R.C. 1997. Petroleum system of the Kutei Basin, Kalimantan, Indonesia. *In*: Proceedings of Petroleum Systems of SE Asia and Australasia Conference, Indonesian Petroleum Association, Jakarta, 709–726.

Raiga-Clemenceau, J., Martin, J.P. & Nicoletis, S. 1988. The concept of acoustic formation factor for accurate porosity determination from sonic transit time data. *The Log Analyst*, **29**, 54–60.

Ramdhan, A.M. & Goulty, N.R. 2010. Overpressure generating mechanisms in the Peciko Field, Kutai Basin, Indonesia. *Petroleum Geoscience*, **16**, 367–376, https://doi.org/10.1144/1354-079309-027

Ramdhan, A.M. & Goulty, N.R. 2011. Overpressure and mudrock compaction in the Lower Kutai Basin – a radical reappraisal. *AAPG Bulletin*, **95**, 1725–1744.

Sargent, C., Goulty N.R., Cicchino, A.M.P. & Ramdhan, A.M. 2015. Budge–Fudge method of pore-pressure estimation from wireline logs with application to Cretaceous mudstones at Haltenbanken. *Petroleum Geoscience*, **21**, 219–232, https://doi.org/10.1144/petgeo2014-088

Schneider, F., Burrus, J. & Wolf, S. 1993. Modelling overpressures by effective-stress/porosity relationships in low-permeability rocks: empirical artifice or physical reality? *In*: Doré, A.G., Augustson, J.H., Hermanrud, C., Stewart, D.J. & Sylta, Ø. (eds) *Basin Modelling: Advances and Applications*. Elsevier, Amsterdam, 333–341.

Skempton, A.W. 1969. The consolidation of clays by gravitational compaction. *Quarterly Journal of the Geological Society, London*, **125**, 373–411, https://doi.org/10.1144/gsjgs.125.1.0373

Środoń, J., Eberl, D.D. & Drits, V.A. 2000. Evolution of fundamental-particle size during illitization of smectite and implications for reaction mechanism. *Clays and Clay Minerals*, **48**, 446–458.

Swarbrick, R.E., Osborne, M.J. & Yardley, G.S. 2002. Comparison of overpressure magnitude resulting from the main generating mechanisms. *In*: Huffman, A.R. & Bowers, G.L. (eds) *Pressure Regimes in Sedimentary Basins and their Prediction*. American Association of Petroleum Geologists, Memoirs, **76**, 1–12.

Teige, G.M.G., Hermanrud, C., Wensaas, L. & Nordgård Bolås, H.M. 2007. Geological constraints of pore pressure detection in shales from seismic data. *Basin Research*, **19**, 33–50.